GSA Data Repository 2017334

The coating layer of glacial polish

Shalev Siman-Tov, Greg M. Stock, Emily E. Brodsky, Joseph C. White

This file includes: supplemental figures, expanded methods, and detailed description of each sample.

Expanded Methods

We documented and sampled glacially polished surfaces in tens of sites along Lyell Canyon and Tuolumne Meadows (Fig. 1B). We conducted detailed analyses on samples collected from three sites: 1) from beneath the Maclure Glacier; 2) in upper Lyell Canyon; and 3) at Daff Dome west of Tuolumne Meadows. We collected the Maclure Glacier sample a few meters inside an ice cave at the toe of the glacier (37°44'50.9"N 119°16'56.3"W; Fig. DR1). The bedrock at this location is composed of metavolanic rock, different from the granodiorite samples collected at lower elevations. We collected the second sample in the upper part of Lyell Canyon two kilometers below the Lyell Glacier (37°45'20.3"N 119°15'35.3"W; Fig. DR2), from granodiorite bedrock of the Kuna Crest facies. We collected the third sample from the southern slope of Daff Dome, west Tuolumne Meadows (37°52'39.37"N 119°24'52.20"W; Fig. DR3), from the Cathedral Peak granodiorite, which is characterized by centimeter-size orthoclase crystals.

We cut the hand-size samples to smaller pieces to fit the electron microscopy stubs (diameter ~ 1 cm). The naturally polished surfaces were coated by a 20-40 nm gold layer and were imaged with scanning electron microscopy (SEM). We obtained surface element maps using energy-dispersive X-ray spectroscopy (EDS) detector. We milled cross-sectional electron transparent samples (foils) perpendicular to the polished surfaces, using focused ion beam (FIB) techniques (Dual-Beam microscope, combined with electron beam FEI Quanta™ 3D field emission microscope). Foil preparation involved depositing additional platinum layers to protect the upper sample from gallium ion beam damage during milling process. Finally, we conducted imaging, diffraction and element analyses using the scanning transmission electron microscopy at 200ke/v (JEOL 2011).

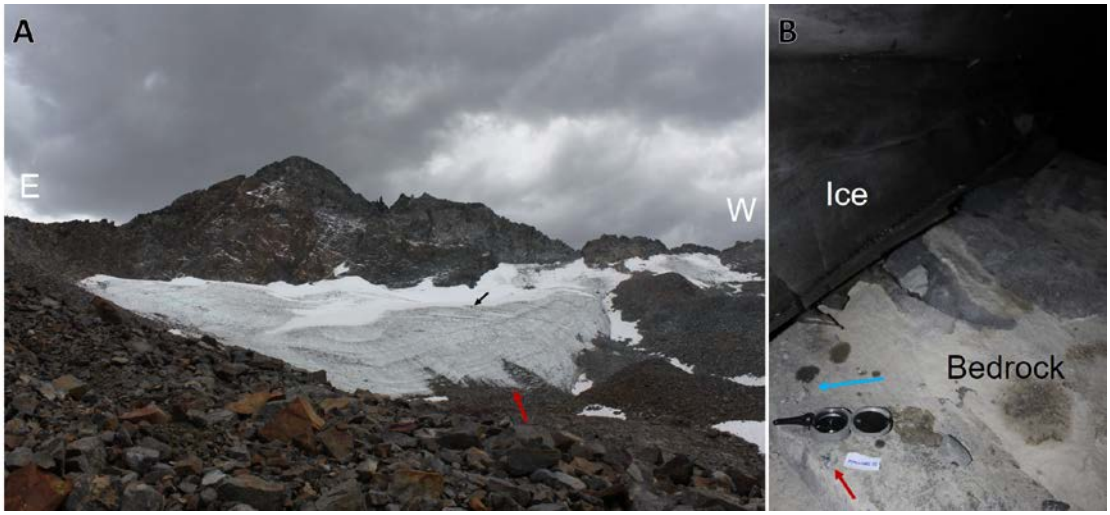

Figure DR1. Maclure Glacier. A: The Maclure Glacier laying on metavolcanic rocks on the northern side of Mount Lyell. The black arrow points to a human for scale, and the red arrow points to the ice cave entrance at the base of the glacier. B: Ice-bedrock contact within the ice cave showing the location where we sampled polished surfaces (denoted by red arrow). Striations suggest the ice flow direction (blue arrow).

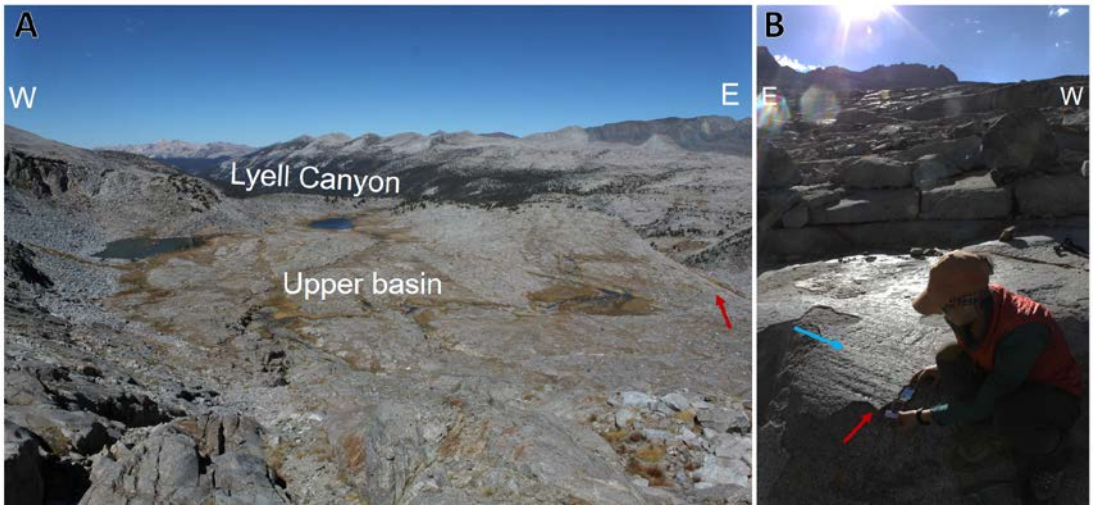

Figure DR2. Lyell Canyon sample. A: The upper basin of Lyell Canyon is 2 km downstream from Lyell Glacier. Many well preserved glacially polished surfaces are exposed on the granodiorite bedrock. B: Sampling location (red arrow) and the ice flow direction (blue arrow) on the polished surface.

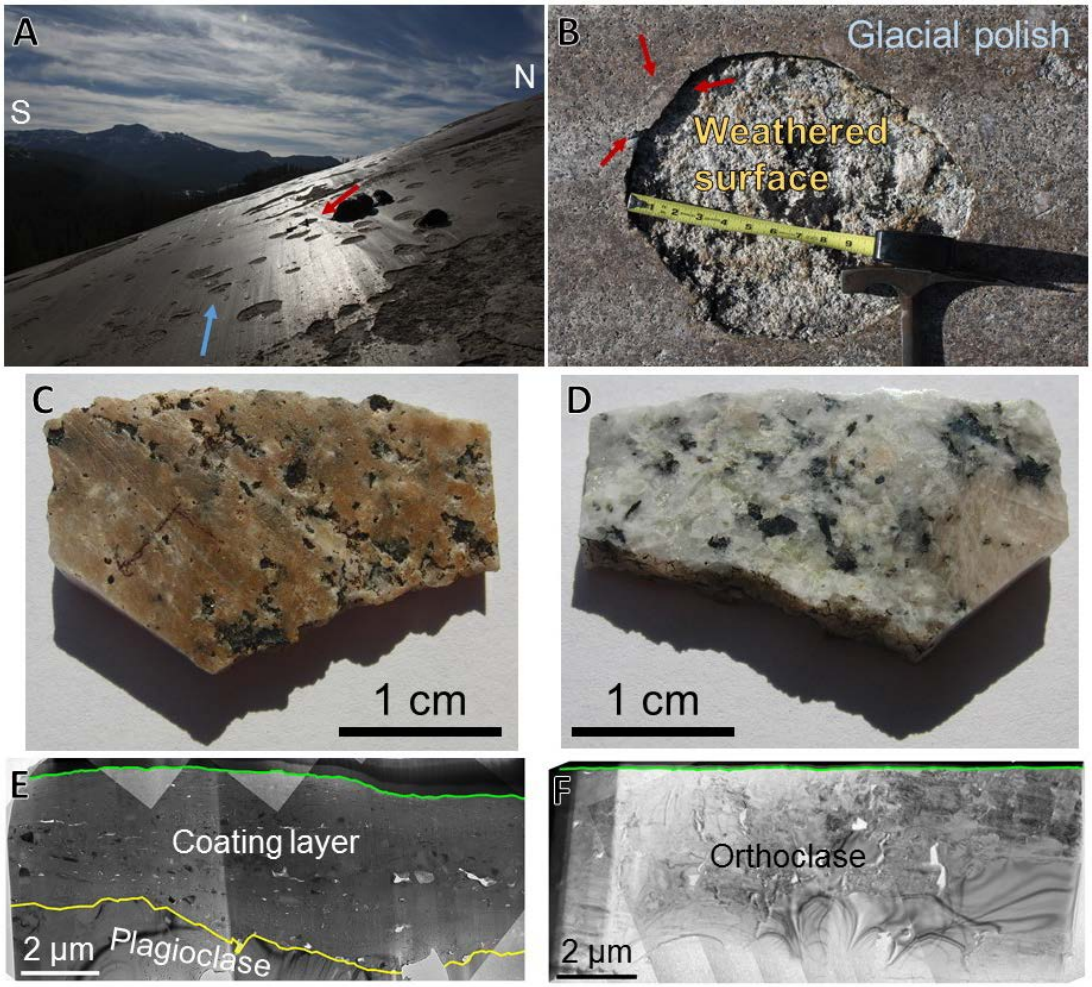

Figure DR3. Daff Dome sample. A: The southern slope of Daff Dome preserves large areas of un-weathered glacial polish on granodiorite bedrock. Ice flow direction is westward in this region (blue arrow). Circular weathering rinds are observed on the polished surfaces and make the sampling easier. B: Sampling location (red arrows) on the margins of one of the circular holes in the glacial polish. The weathered rock is much rougher compare to the glacial polish. C: Glacial polish sample with striations. The polished surfaces are brown relative to the gray color of the granodiorite bedrock. It is difficult to distinguish between the granodiorite minerals as the coating is partly opaque. D: Manual polish of the other side of the natural sample (from C). The smooth surface is transparent allowing easy mineral identification. E: TEM image of a cross section of the naturally polished sample (from C). The coating layer caps the abraded surface (yellow line) makes the surface smoother (green line). F: TEM image of a cross section of the manually polished sample (from D). The optically smooth surface (green line) is also the abraded surface, no coating layer observed at that scale.

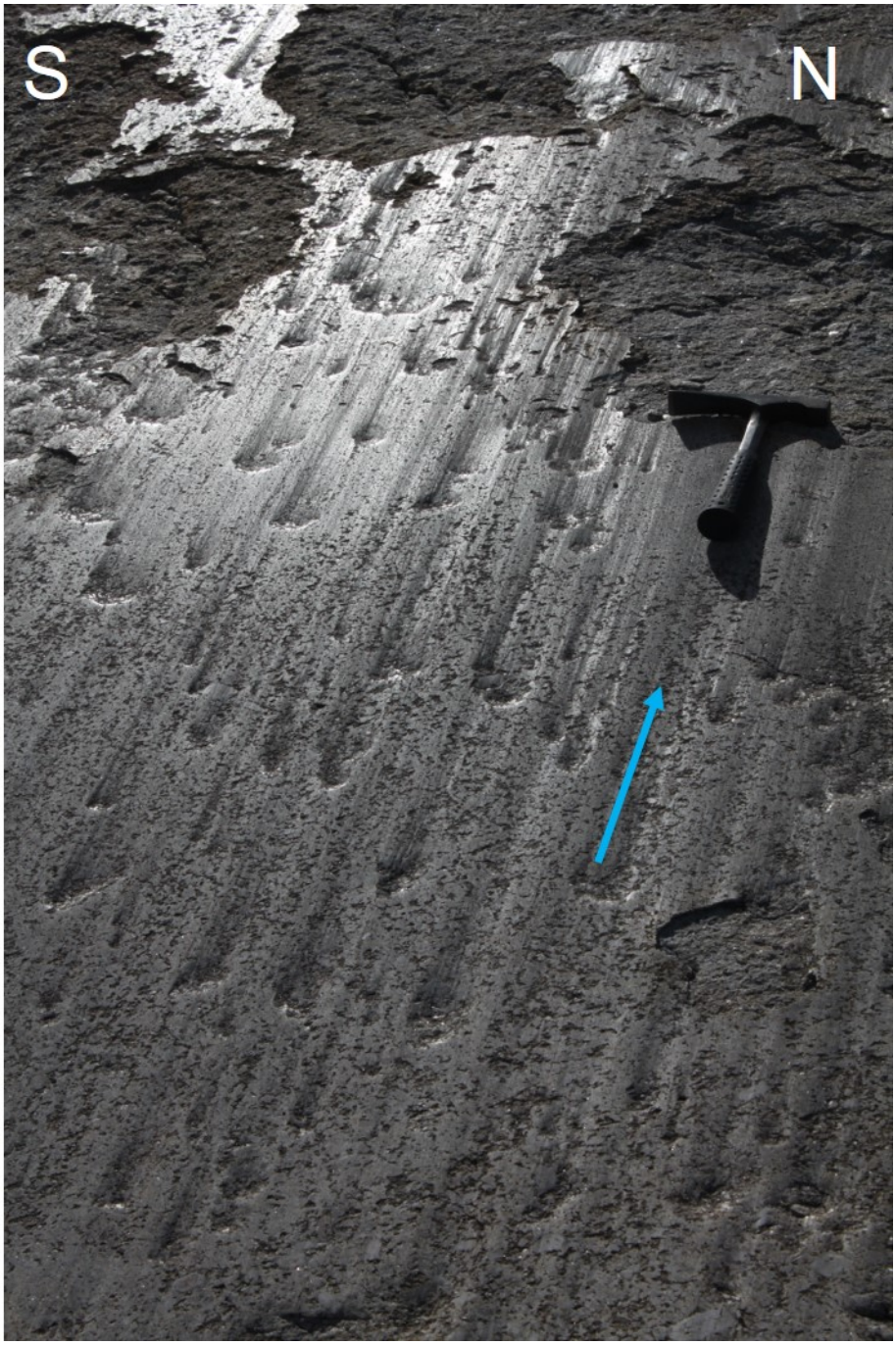

Figure DR4. Striated glacial polish on the eastern slope of pothole dome. The striation inner part is also polished, possibly suggesting that they were smoothed after their formation. These striations point on the direction of ice slip from the small circular dipression towards their sharp end (blue arrow illustrating the direction). Rougher, weathered surfaces are not shiny.

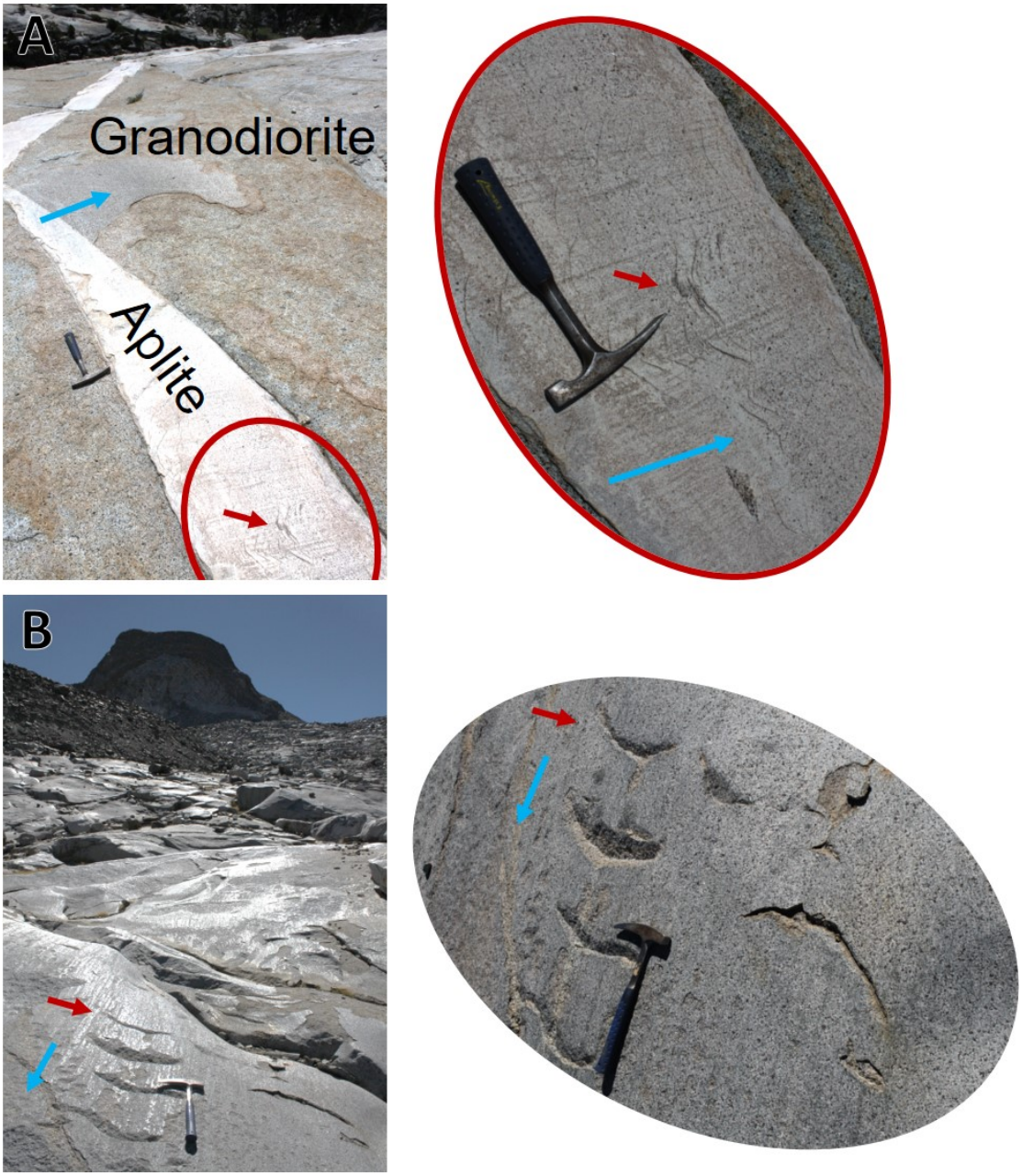

Figure DR5. Crescentic fractures. A: Chatter marks on a polished aplite dike (red arrows) agree with the mapped ice flow direction (blue arrow). They are concave up toward the ice sliding direction. B: Crescentic gouges (red arrows) are concave in both directions but always in perpendicular to the striations (blue arrows).

Additional sample descriptions

The Maclure Glacier

For the ice cave sample, an original amphibole crystal is fractured and bent toward the surface (Fig. 2A). The amphibole cleavage planes, i.e. {110}, in the inner part of the crystal (below the red line in Fig. 2A) are oriented almost perpendicular to the surface (green line). The outer part of this amphibole (above the red line in Fig. 2A) bends toward the ice flow direction. The bending angle changes laterally (across the section), but consistently increases toward the surface, and up to ~60° from the original orientation (Fig. 2B). Moreover, the fracture density in the bent region increases toward the sample surface. The crystal is fractured both along the cleavage planes and sub-perpendicular to them, allowing the *in-situ* formation of new elongated grains (Fig. 2C). The nanograin size decreases toward the surface until it is impossible to resolve any crystalline structure by electron diffraction (between the green and the yellow lines in Figs. 2B-2C).

A non-uniform-thick coating layer is observed on top of the abraded surface (between the yellow and the green line in Fig. 2). This irregular coating may imply the sample is in the early stages of the coating layer formation. In general, a continuous layer, 10's – 100's nm thick, is observed underneath the artificial gold and platinum coatings, caps the damaged amphibole crystal (Figs. 2A-2D). This coating comprises amorphous material, nano-crystals, and a few larger-fragments. On one end of this sample the coating is thicker, comprising nano-size fragments in a grain-supported breccia (Fig. 2D). The breccia thickness is ~1 μm and its thickness is similar to the thickness of the adjacent damaged layer (between the red and the green lines in Fig. 2A). The fragments are in general angular, mostly amphibole grains, with some foreign fragments that were transported a distance which is larger than the foil dimension. The amphibole fragments are rotated compare to the original crystal orientation, suggesting the displacement and rolling of clasts in addition to in-situ fragmentation of the damaged crystal. The void space (white) between the fragments suggest that no matrix filled the inter-clast voids (bright field TEM imaging), differently from the other coatings described below that comprise amorphous matrix. On the right end of this foil the coating patch comprises 100 nm-size amorphous silica fragments, tens of nanometer crystals of amphibole and other indeterminate phases

(possibly neo-crystalline quartz), and amorphous material presumably filling the voids (Figs. 2A and 2E).

Daff Dome

The coating layer of the Daff Dome sample has a composite structure consisting of an outer phyllosilicate layer with inner layers comprising sub-micrometer fragments within an amorphous matrix (Fig. 3A). The coating layers have a total thickness of 3.2 to 4.6 µm and cap an abraded plagioclase crystal. This several micrometer-thick layer may account for the partial opacity of some of the glacially polished surfaces (Fig. DR3C). The phyllosilicate layer is 0.3 - 1.0 µm thick, similar to the coating of the Lyell Canyon sample. This layer comprises illite crystals embedded within amorphous silica with minor amount of Al, Mg, Fe and Ca. In contrary to the Lyell Canyon upper basin sample, we observe no regions of pure amorphous material (mottled texture in Fig. 3C) along this phyllosilicate layer. Under the phyllosilicate layer, three layers can be distinguished, each having a similar texture of rock fragments within amorphous material (Fig. 3A). The bottom layer, lying adjacent to the abraded plagioclase, is unique in having a silica rich, amorphous matrix, with very minor aluminum. The center layer is enriched in fragments characteristic of the granodiorite mineralogy. The amorphous matrix of this layer contains aluminum in addition to silica. The upper layer, underlaying the phyllosilicate layer, has a similar amorphous matrix with fewer clasts. It is defined as a separate layer, as a vein that cuts through the two lower layers does not pass through this upper layer (Fig. DR7). Moreover, no offset is observed for the broken clasts along this linear vein, suggesting that the matrix and fragments have similar hardness when fractured. Some of the clasts in these three layers seem to be clustered by mineral type (same outline color in Fig. 3A). The clast size within these clusters decreases with the ice flow direction, suggesting fragmentation and smearing of the coating during shear. The four layers observed in the Daff Dome coating imply a complicated formation process that could include several stages during its genesis.

Lyell Canyon upper basin

Cross sections of the Lyell Canyon sample show a 0.4 to 1.2 µm thick coating layer that caps an orthoclase crystal (Figs. 3B and DR6). The layer mostly contains nano-sized sheet-silicate minerals embedded in amorphous matrix with a few rounded clasts (Figs. 3B-3D and DR6). Diffraction patterns and element analysis demonstrate

that the elongated crystals are phyllosilicates comprising well-formed grains of Fe(Mg) chlorite and more diffuse aggregates of illite. The occurrence of low-temperature smectitic clays or common alteration phases could not be confirmed by combined diffraction and elemental analysis in STEM.

These composition and structures were observed for the two cross-sections cut parallel (Fig. 3B-3D) and perpendicular (Fig. DR6) to surface striations. The phyllosilicates exhibit a foliation sub-parallel to the sample surface (Figs. 3C-3D). These grains seem to flow around isolated fragments forming an anastomosing flow-like texture (Fig. 3D). S/C shear fabric, are possibly observed in the phyllosilicate layer (Fig. 3C). Elongated regions of amorphous material are observed within the phyllosilicate coating (Figs. 3B and DR6A). These regions have a mottled texture and with elemental analyses dominated by silicon, aluminum, and oxygen (Fig. 3C).

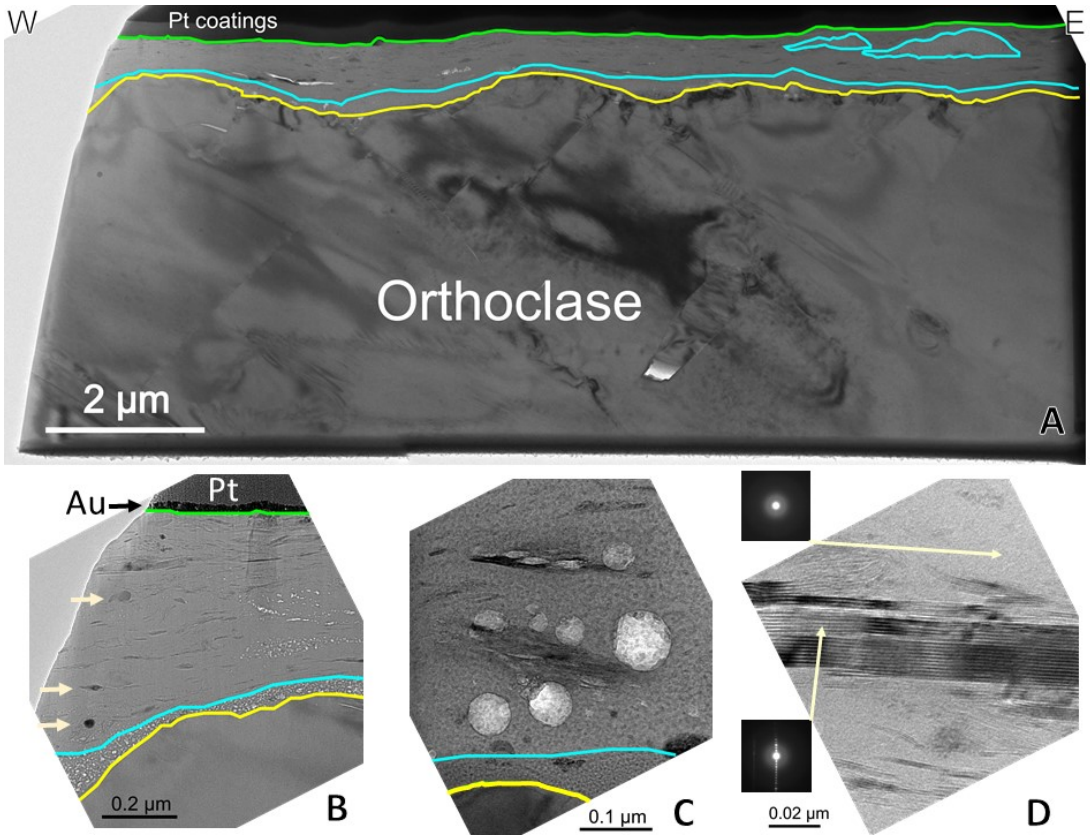

Figure DR6. A cross section of glacial polish sample from the upper basin of Lyell Canyon. This sample cut in perpendicular to the striation orientation. Glacial polish surface (green line) is smoother than the inner abraded surface of the orthoclase crystal (yellow line). Elongated domains of amorphous silica are found within the phyllosilicate coating layer (outlined by blue). B to D, are zooming in images of different locations along the coating layer shown in A. B: Artificial gold (black) and platinum (dark gray) coatings were deposited on the glacial polish sample (green line). The natural coating is mostly composed of nano-sized phyllosilicate crystals with a few rounded particles (light color arrows). C: Phyllosilicate minerals in the coating (light circles caused by beam damage during TEM imaging). D: A chlorite crystal. In its middle, clear parallel lines, i.e. crystal planes are observed (diffraction pattern at bottom left), while its margins are less ordered and may denote on weathering of the crystal. The crystal is surrounded by amorphous matrix (upper left diffraction pattern).

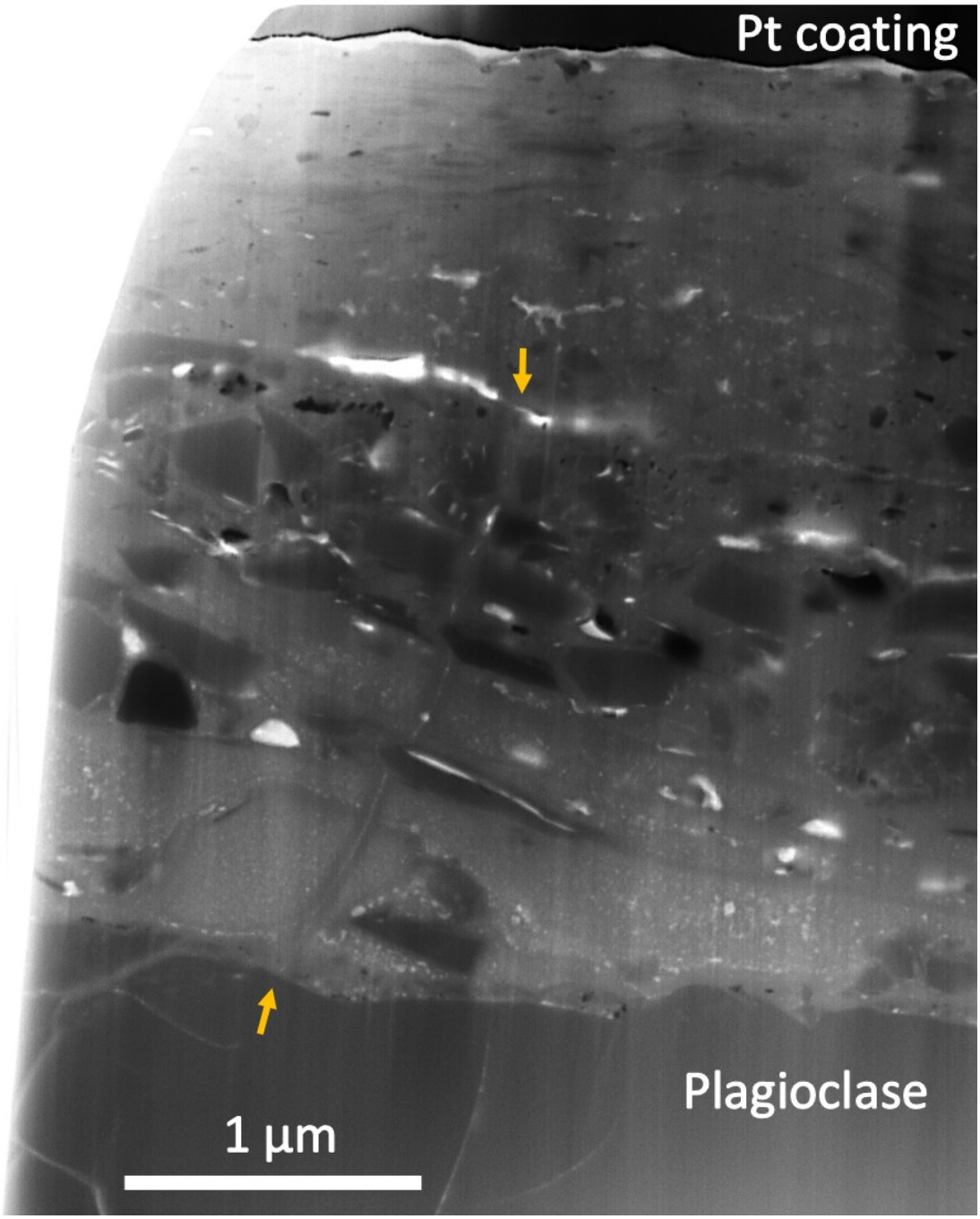

Figure DR7. Zooming to the left side of Daff Dome cross sectional foil presented in Fig. 3A. The four coating sub-layers are clearly observed on top of the plagioclase abraded crystal. A vein (marked by two arrows) cut through the two lower sub-layers. The vein, fractured both, the amorphous material and different fragments. It seems that the same material comprises the vein, was injected into fractures within the plagioclase (left of the lower arrow).